EPJ E
Soft Matter and Biological Physics
EPJ.org
your physics journal

Eur. Phys. J. E **30**, 283–290 (2009)   DOI: 10.1140/epje/i2009-10526-3

On a moving liquid film and its instability on textured surfaces

M. Hamamoto-Kurosaki and K. Okumura

EDP SCIENCES
Società Italiana di Fisica
Springer

Eur. Phys. J. E **30**, 283–290 (2009)
DOI 10.1140/epje/i2009-10526-3

THE EUROPEAN PHYSICAL JOURNAL E

Regular Article

On a moving liquid film and its instability on textured surfaces

M. Hamamoto-Kurosaki and K. Okumura[a]

Department of Physics, Graduate School of Ochanomizu University, 2-1-1, Otsuka, Bunkyo-ku, Tokyo 112-8610, Japan

Received 25 May 2009 and Received in final form 16 September 2009
Published online: 24 October 2009 –

Abstract. Recently, two regimes of viscous friction on textured surfaces were proposed in the context of penetration of liquid film into the texture (EPL **79**, 56005 (2007)): the Poiseuille and Stokes regimes. With this idea on viscous friction, we theoretically discuss instabilities on a liquid film on textured surfaces when the film is forced to move with external forces. When a film recedes due to a pressure drop, we find scaling laws for instabilities to be checked in future experiments. When a circular film expands due to centrifugal force we find that the expanding film is stable against rim fluctuations (within the linear stability analysis) with its radius determined by a simple equation. Our discussion sheds light on the curvature of the front of the moving liquid film on textured surfaces and how the film thickness is kept fixed to the texture height on textured surfaces, aspects which have not been discussed in previous studies.

PACS. 68.08.Bc Wetting – 47.20.Ma Interfacial instabilities (*e.g.*, Rayleigh-Taylor)

1 Introduction

It has become possible to make regular patterns on nano to submicron scale on substrates. Characterization of wettability of such surfaces has been actively studied (*e.g.*, [1–7]). One important issue has been wetting transition of a drop deposited on such surfaces, *e.g.*, from the Cassie state (in which air is trapped between the drop bottom and the surface) to the Wenzel state (in which liquid penetrates and replaces the air in the Cassie state); some aspects on this are discussed, for example, in [8–16].

Another issue of interest should be imbibition: liquid spontaneously penetrates into the texture just as we put a piece of tissue paper in contact with a coffee. Recently, the dynamics of such imbibition on surfaces textured with forest of pillars of height h has been studied [17] where the radius of a pillar and the interspacing between two adjacent pillars are b and l, respectively (see fig. 1).

The experimental results of imbibition were consistent with the assumption of two regimes of viscous friction: Poiseuille and Stokes regimes. The former appears when the film thickness is small ($h < l$) where we can regard that a thin film of thickness h (equal to the pillar height) is advancing on a textured surface: velocity distribution is parabolic with velocity zero at the substrate bottom and at the maximum on the film surface as in a typical Poiseuille flow. The latter Stokes regime is appropriate when the film thickness is large ($h > l$) where we can regard that the film of thickness h feels friction from each cylindrical pillar with the pillars well separated ($b \ll l$).

[a] e-mail: okumura@phys.ocha.ac.jp

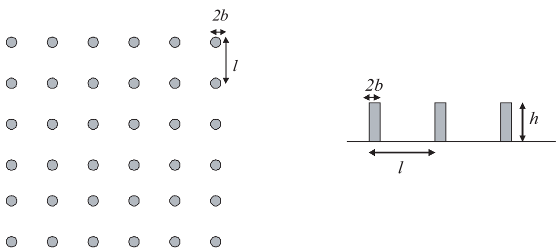

Fig. 1. Geometry of textured surface: top view on the left and side view on the right.

In this paper, based on these two regimes of friction, we discuss instabilities associated with a liquid film whose thickness is kept fixed to h due to pillars, via linear-stability analysis with simple scaling arguments to clarify the physics behind the mathematical analysis. As a result, we find some predictions which might be tested in future experiments.

We think that the important message of the experiment in [17] is the fact that, at least for explanation of macroscopic dynamics, we can neglect local deformation of the film surface around pillars (except for a moving edge) with pillar height h determining the thickness of the film. This point is examined in more detail by providing original arguments in the next section.

However, as becoming clear in the next section, this simplification occurs only when the pillar height h and the inter-distance l are larger than the pillar radius b and when these parameters are smaller than the capillary length. In addition, the dimension of the film area considered is much

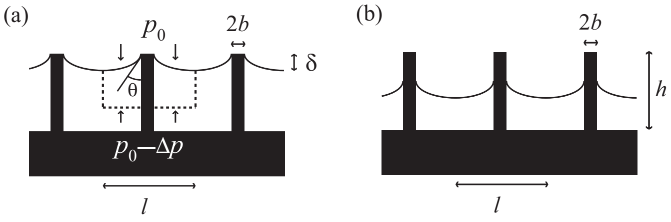

Fig. 2. Microscopic views on a film on a textured substrate. (a) A film pinned by the top edges of pillars. (b) A film not pinned by the edges.

larger than the texture scale where a continuum description of the texture is possible. In fact, these parameters in [17] are summarized as $b = 2\,\mu$m, $h = 10$–$20\,\mu$m, and $l = 10\,\mu$m, while the penetration length of the film is of the order of millimeters, and thus the required conditions are satisfied approximately (since the surface tension γ of the oil used in [17] is about 20 mN/m, the important quantity p_c introduced below is a few kPa). We remind here that the analysis of the present paper is applicable only when these conditions are met.

2 Microscopic deformation of the film surface

We consider a film on a textured substrate pinned by the top edge of pillars (fig. 2a). At the edge the angle θ can take an arbitrary value in the range

$$\theta_E < \theta < \theta_E + \pi/2, \tag{1}$$

where θ_E is the contact angle, without violating the local force balance at the contact line, *i.e.*, Young's relation,

$$\gamma \cos\theta_E = \gamma_S - \gamma_{SL}, \tag{2}$$

where γ, γ_S, and γ_{SL} are the interfacial energies between liquid-air, solid-air, and solid-liquid, respectively. A more global force balance (in the quasi-static limit) of the portion of liquid enclosed by the dashed line and the liquid surface in fig. 2a leads to a relation

$$2\pi b\gamma\cos\theta = l^2 \Delta p, \tag{3}$$

when the inside pressure is $p_0 - \Delta p$ (the effect of gravity can be neglected since h is much smaller than the capillary length). In other words, when the inside pressure is the same as the outside pressure p_0 the surface should be flat, *i.e.*, $\theta = \pi/2$, where the liquid-air surface area becomes minimum. In addition, the pressure difference Δp should be in the range $p_c \cos\theta_E < \Delta p < p_c \sin\theta_E$, where

$$p_c = 2\pi\gamma b/l^2, \tag{4}$$

because of eq. (1). If the pressure difference is outside of the above range, the film cannot exist because the quasi-static force balance cannot be attained.

When a film is not pinned at the edge of pillars as in fig. 2b the global balance is possible only when $\Delta p = p_c$ while the surface energy decreases as the pinning height gets closer to the maximum height (*i.e.*, the pillar height, h). This is because if we compare panels a) and b) of fig. 2, the extra solid-air surfaces of the top part of pillars are covered and replaced by solid-liquid interfaces with the replacement energy $\gamma_{SL} - \gamma_S$ per unit area, which is negative when the contact angle θ_E is less than $\pi/2$ due to Young's relation in eq. (2). Thus, *the film should be pinned at the edge of pillars* to minimize the surface energy.

The pressure difference Δp can be interpreted as the Laplace's pressure jump γC, where C is the curvature of the surface. In this case the curvature of the surface is given by $2\pi b\cos\theta/l^2$, which is at most $2\pi b/l^2$. The small dent δ in the middle between the pillars (fig. 2a) scales as $Cl^2 \sim b$. *The film thickness on the textured substrate can be assumed to be* h, because $h \gg b$.

When we take the effect of contact hysteresis into account, eq. (1) is changed to $\theta_r < \theta < \theta_a + \pi/2$, where θ_r and θ_a are the receding and advancing angles, respectively, but the physical essence remains intact. In the following, however, for definiteness and for simplicity, we assume that the contact angle is zero where a microscopic wetting film is expected ahead of the macroscopic contact line and, thus, there is no effect of contact angle hysteresis.

In summary, 1) the film is pinned at the edge of pillars, 2) the surface of the film adjusts its microscopic shape by changing θ to be compatible with the pressure difference Δp, 3) the average film thickness can be still assumed to be h, and 4) the inside pressure p of the film should be in the range

$$p_0 - p_c < p < p_0, \tag{5}$$

otherwise, the film cannot exist (note that a film of molecular thickness can exist).

These statements suggest that the curvature at the advancing front of a film on a textured substrate should be given by

$$C_0 = 2\pi b/l^2 \tag{6}$$

and the boundary condition at the advancing front of the film should be given by

$$p = p_0 - p_c \text{ at the advancing front.} \tag{7}$$

Here, the advancing front implies that the pressure decreases as we approach the front along the moving direction and the pressure drop drives the film. As a matter of fact, in the previous theory of penetration the pressure at the moving front can be shown to be $p_0 - p_c$ (see appendix A), which is consistent with the condition in eq. (5).

Based on these consideration and on the support by the previous work [17], we assume that the film on textured surfaces is fixed to a constant h in the following macroscopic discussions.

3 Instability of a receding film on textured surfaces

We consider a liquid film of thickness h on a textured surface on the horizontal x-y plane receding in the "$+x$"

direction (the pillar's bottom and top are located at $z = 0$ and $z = h$, respectively): at the initial time $t = 0$, the liquid occupies the region $x > 0$ and the liquid-air interface (receding edge) placed at $x = 0$ is moving in the "$+x$" direction with speed U. The instability of the receding edge (the liquid-air interface) is the problem. Experimentally, this can be realized by absorbing a liquid film on a textured surface at one end in a controlled way (we do not have to attain a time-independent U; see sect. 5).

We can deal with this situation by extending the discussion of Saffman and Taylor [18]. We discuss below only physical essences through naive scaling arguments, while a complete mathematical derivation is given in sect. 5. We stress here that the purpose of the discussions below is not to present a fully justifiable derivation, but rather, to provide a possible physical interpretation of the mathematical analysis in sect. 5.

Let us first discuss viscous friction associated with liquid motion. Around the pillars (at least at places remote from pillars), the flow generates velocity gradients over a distance h, as in the Poiseuille flow inside a thin film, which results in a friction between the moving liquid of thickness h and the bottom solid surface. This (average) friction f_1 acting on the bottom of a film element of volume $h\mathrm{d}x\mathrm{d}y$ scales as

$$f_1 \sim -(\eta U/h)\mathrm{d}x\mathrm{d}y \tag{8}$$

(if pillars are not too dense).

Near a pillar, a film element is dragged by pillars; a pillar causes a friction force to the fluid just as a sphere in a flow does. For such a Stokes flow, velocity gradients exist over a distance around b (the pillar radius) and the friction of the order of $\eta U/b$ per unit area takes place on the surface $2\pi bh$ of a pillar, from which we obtain a force f_2 acting on the film element of volume $h\mathrm{d}x\mathrm{d}y$ scaling as the quantity, $(\eta U/b)\cdot bh$ multiplied by the number of the pillars in the element $\mathrm{d}x\mathrm{d}y/l^2$:

$$f_2 \sim -(\eta U h/l^2)\mathrm{d}x\mathrm{d}y. \tag{9}$$

More exactly, the force per unit length of pillar in this Stokes friction, $-\eta U$, comes with an extra numerical prefactor which contains weak logarithmic dependence on physical parameters: *e.g.*, in the case of an infinite cylinder the factor contains a term $\ln[\eta/(bU\rho)]$ with ρ the liquid density, in the case of a finite cylinder of length h a term $\ln(h/b)$, and in the case of regularly spaced (with a distance l) cylinders of infinite length a term $\ln(l/b)$ [19,20].

Comparing these two friction forces ($f_1/f_2 \sim l^2/h^2$) we find two distinctive regimes: 1) For short pillars ($h < l$), the Poiseuille friction at the film bottom is dominant and 2) for long pillars ($h > l$) the Stokes friction from pillar surfaces is dominant.

The friction $f_1 + f_2$ acting on the film element of volume $h\mathrm{d}x\mathrm{d}y$ is balanced by a force, $[p(x) - p(x + \mathrm{d}x)]h\mathrm{d}y$, originating from the pressure difference in the flow direction, *i.e.*, in the x-direction (we are interested in time scales where the initial inertial dynamics is over). We find Darcy's law in the two regimes

$$\vec{U} = -\kappa\vec{\nabla}p, \tag{10}$$

where

$$\kappa = \begin{cases} h^2/(3\eta), & h < l, \\ \sim l^2/\eta, & h > l. \end{cases} \tag{11}$$

In the case of the original discussion by Saffman and Taylor, they considered a Hele-Shaw cell of thickness h where the coefficient 1/3 in eq. (11) is replaced with 1/12 because in the present case the appropriate boundary condition for velocity at the film upper free surface is not $v = 0$ but $\partial v/\partial z = 0$.

Once Darcy's law is established, we can discuss the physical origin of instability when a small disturbance is created at the liquid-air interface: the small disturbance on the receding edge line tends to be enhanced under Darcy's law. To understand this, let us neglect the pressure jump at the liquid-air interface originating from surface tension and clarify the effect of the viscous force. When there is no disturbance on the receding edge line described by $x = 0$ at $t = 0$, the pressure inside the liquid at the position x is simply given by

$$p = p_0 - (U/\kappa)x, \tag{12}$$

where p_0 and U/κ are the atmospheric pressure and a pressure gradient $\partial p/\partial x$ (which is a constant for x), respectively. By considering the case when the interface is deformed in the shape given by $x = \varepsilon\cos(2\pi y/\lambda)$ at $t = 0$, we find, for example, at $y = 0$, that the receding edge is located at $x = \varepsilon$ and the pressure on the left (p_0) is higher than that on the right ($p_0 - U\varepsilon/\kappa$) so that the receding edge tends to move in the right direction; at $y = \lambda/2$, on the contrary, the receding edge located at $x = -\varepsilon$ and the pressure on the left is lower than on the right so that the receding edge tends to move in the opposite direction; the sinusoidal receding edge curve is unstable and tends to be more deformed because of Darcy's law. Note that, if the film is advancing (in the "$-x$" direction) instead of receding (in the "$+x$" direction), this effect of viscosity tends to stabilize the disturbance and thus instability occurs only for receding films; for example, since for an advancing film (in the "$-x$" direction) U is in the opposite direction, *i.e.*, the minus sign in eq. (12) is replaced with the plus, at $y = 0$, the advancing front is located at $x = \varepsilon$ and the pressure on the right ($p_0 + U\varepsilon/\kappa$) is higher than that on left (p_0), so that the advancing front tends to move in the left direction: the advancing front tends to be stabilized. This is the reason why instability is not observed in the previous experiment [17].

Contrary to viscosity, capillarity always tends to stabilize the disturbance because any deformation of the line implies an increase of the liquid-air interface of height h (whose interfacial energy is γ). The interface element located from $y = -\lambda/2$ to $y = \lambda/2$ is subject to surface tension of magnitude γh at the two edges (of length h) whose x component scales as $-\gamma h\varepsilon/\lambda$ and tends to move in the left direction; the adjacent elements tend to move in the opposite direction such that the receding edge tends to return to a straight line. In terms of pressure, this tendency is evaluated as $\sim \gamma\varepsilon/\lambda^2$ (the force $\sim \gamma h\varepsilon/\lambda$ acting on one element divided by the area $\sim h\lambda$), which scales as the Laplace pressure $\sim \gamma\varepsilon/\lambda^2$ as expected. Note that the contribution from the second curvature of the order of the film thickness h is unchanged before and after this small deviation ε, so that we can neglect this contribution from the present argument.

Comparing these two factors, viscosity which tends to enhance the disturbance and surface energy which tends to suppress the disturbance, we have a criterion for instability in terms of pressure: $U\varepsilon/\kappa \gtrsim \gamma\varepsilon/\lambda^2$, which reduces to

$$\lambda \gtrsim \lambda_c, \tag{13}$$

with

$$\lambda_c \equiv \left(\frac{\gamma}{\eta U}\right)^{1/2} L; \qquad L = \begin{cases} h, & h < l, \\ l, & h > l, \end{cases} \tag{14}$$

where L is h in the Poiseuille regime and l in the Stokes regime. If the wavelength is longer than λ_c, the disturbance is enhanced while it is suppressed in the opposite case.

In reality, small disturbance is not created in a simple form such as $x = \varepsilon\cos(2\pi y/\lambda)$, but in a complex form expressed by superposition of these simple forms, out of which the mode with the fastest growing speed survives. This fastest mode gives the characteristic length scale to be compared with experiments. By doing the standard linear stability analysis, we can determine the fastest mode as, for example, $\lambda^* = 2\pi\sqrt{3}\lambda_c$, in the Poiseuille regime (see sect. 5). We can confirm explicitly, at least for examples given in this paper, that the onset length of the instability λ_c and the wavelength of the fastest mode λ^* are different only with a numerical pre-factor; for experimental confirmation of the scaling relations, both quantities are identical. Because of this reason we identify λ_c with λ^* in this paper.

Equation (14) is one of the scaling laws to be compared with experiments. For typical parameters (*e.g.*, $\eta = 10\,\mathrm{mPa\,s}$, $\gamma = 20\,\mathrm{mN/m}$, $U = 0.2\,\mathrm{mm/s}$, and h or $l \sim 10\,\mu\mathrm{m}$), λ_c is of the order of mm.

In the present case of receding film, the pressure inside the liquid decreases as we go away from the receding edge in the x-direction, so that it may be possible that pillars are no longer able to keep the thickness h considering the discussion in sect. 2; this may happen $x = x_c$, with $Ux_c/\kappa \simeq p_c$. Typical value of $x_c \simeq 2\pi b\gamma/(\eta U)$ for $h \sim l$ is around $0.1\,\mathrm{m}$ where gravity comes into play (*e.g.*, $\eta = 10\,\mathrm{mPa\,s}$, $b = 2\,\mu\mathrm{m}$, $\gamma = 20\,\mathrm{mN/m}$ and $U = 0.2\,\mathrm{mm/s}$) so that this effect does not affect the analysis of instability in sect. 3 (and similarly in sect. 4 below).

4 Instability of a circular growing hole in a film on textured surfaces

In this section, we consider a case where the straight-line interface in the previous section is replaced with a circular interface. In this case, we find the same Darcy's law. On the r-θ plane the pressure acting on a film element of volume $hr\mathrm{d}\theta\mathrm{d}r$ in the r-direction is given by $p(r)h\mathrm{d}\theta - p(r+\mathrm{d}r)h(r+\mathrm{d}r)\mathrm{d}\theta + p\mathrm{d}\theta h\mathrm{d}r$ (with the last term being the contribution acting on the two sides (of area $h\mathrm{d}r$) of the volume element), which reduces to $-(\partial p/\partial r)\mathrm{d}rh\mathrm{d}\theta$; the force balance, for example, in the Poiseuille regime is given by

$$-(\partial p/\partial r)h\mathrm{d}\theta - (\eta U/h)r\mathrm{d}\theta\mathrm{d}r \simeq 0, \tag{15}$$

which reduces to eq. (10). In a similar way, we recover eq. (10) also in the Stokes regime.

When we describe the initial circular interface by $r = R$ at $t = 0$, due to the incompressibility of the liquid the flow flux $Q = 2\pi rUh$ should be a constant for spatial coordinates; the velocity U is now dependent on spatial coordinates: by noting that U at $r = R$ in this case can be expressed as $\dot{R}$, we obtain

$$U = \dot{R}\frac{R}{r} = \frac{Q}{2\pi rh}\,, \tag{16}$$

with Q and h independent of spatial coordinates. From eqs. (10) and (16), the pressure inside the liquid at a position r is simply given by

$$p = p_0 + \frac{\dot{R}}{\kappa}R\log\frac{R}{r}\,, \tag{17}$$

where p_0 is the atmospheric pressure, if we neglect the pressure jump at the liquid-air interface originating from surface tension. Note that in the ensuing analysis $R(t)$ can be a general function of t (see sect. 5). Let us consider a case when the interface is deformed in the shape given by $r = R + \varepsilon(t)\cos(n\theta)$ at $t = 0$, where the wavelength λ is defined by

$$\lambda = 2\pi R/n; \tag{18}$$

for example, at $\theta = 0$, the receding edge (in the "$+r$" direction) is located at $r = R + \varepsilon$ and the pressure on the inside (p_0) is higher than that on the outside ($p_0 - \dot{R}\varepsilon/\kappa$, *i.e.*, eq. (17) at $r = R + \varepsilon$), so that the receding edge tends to move in the outside direction; at $\theta = \pi/n$, on the contrary, the receding edge located at $r = R - \varepsilon$ and the pressure on the inside is lower than on the outside, so that the receding edge tends to move in the opposite direction; the sinusoidal receding edge curve is unstable and tends to be more deformed because of Darcy's law. The surface energy tends to stabilize the disturbance as before. The tendency in terms of pressure $\gamma\varepsilon/\lambda^2$ in the previous section is unchanged with $\lambda = 2\pi R/n$, when $\lambda \ll R$ (*i.e.*, $n \gg 1$). Thus, just as before, viscosity tends to enhance the disturbance and surface energy tends to suppress the disturbance; comparing these effects in terms of pressure, we have the same criteria for instability: $\dot{R}\varepsilon/\kappa \simeq \gamma\varepsilon/\lambda^2$, which results in eq. (14) with regarding U as $\dot{R}$; from eq. (18) the fastest mode is given by an integer closest to

$$n_c \simeq \left(\frac{\eta\dot{R}}{\gamma}\right)^{1/2}\frac{R}{L} \simeq \left(\frac{\eta QR}{\gamma}\right)^{1/2}\frac{1}{L}\,, \tag{19}$$

where L is h in the Poiseuille regime and l in the Stokes regime. Note that the number of fingers scales as eq. (19).

The above expression is valid for $n \gg 1$ (see sect. 5); for the previous typical parameter set, $n_c \simeq 10$ when we start with an initial radius $R \simeq 1\,\mathrm{cm}$.

We might consider that dewetting of a liquid film on a textured surface would correspond to the situation considered here but this may not be correct; according to the standard theory of dewetting film [1], the moving part of the film is essentially a rim around the circular hole created as a result of accumulation of dewetted film, so that virtually no Poiseuille flow is developed in the film far from the rim. However, the instability of the dewetting rim on the textured surface should be surely an important problem.

5 Instability of spin coating on textured surfaces

In this section we consider instability of a circular interface which is forced to expand by centrifugal force due to rotation of the textured surface. We start discussing this case of spin coating in the Poiseuille regime, which is generalized immediately for the Stokes regime. Although in sects. 3 and 4 we limit ourselves to scaling arguments, in this section we give a more mathematical account: the linear-stability analysis of spin coating discussed here practically includes the cases discussed in sects. 3 and 4 as shown below.

The density and viscosity of air are neglected against those of the liquid (ρ and η); we consider only the flow of the liquid. The liquid follows the Navier-Stokes equation in the frame rotating with an angular velocity vector $\vec{\omega}$

$$\rho\left(\frac{D\vec{v}}{Dt}+\vec{\omega}\times\vec{v}+\vec{\omega}\times(\vec{\omega}\times\vec{r})\right)=-\vec{\nabla}p+\eta\nabla^2\vec{v}. \quad (20)$$

In the lubricant approximation the first inertial term on the left-hand side is neglected compared with the second viscous term on the right-hand side. The second Coriolis term on the left-hand side is neglected against the third centrifugal term because the ratio $\sim v/(\omega r)$ is small when the velocity in the rotating frame $\vec{v}$ is small compared with the rotational speed $r\omega$. With this set of approximation, we find that the height-averaged velocity $\vec{U}$ satisfies $3\eta\vec{U}/h^2=\rho\omega^2\vec{r}-\vec{\nabla}p$, with $\vec{\nabla}p$ being z-independent; in the standard treatment of spin coating [21] or rotating Hele-Shaw cell [22,23] all the quantities are made z-independent by taking average when needed. This is generalized for spin coating on textured surfaces both in the Poiseuille and Stokes regimes by using κ in eq. (11)

$$\vec{U}/\kappa=\rho\omega^2\vec{r}-\vec{\nabla}p. \quad (21)$$

The velocity in eq. (21) can be generated from a potential $\vec{U}=\vec{\nabla}\phi$, with

$$\phi=-\kappa\left(p-\frac{1}{2}\rho\omega^2r^2\right). \quad (22)$$

The equation of the conservation of the flow $\partial h/\partial t+\vec{\nabla}\cdot(h\vec{U})=0$ reduces to an incompressibility equation for the averaged velocity $\vec{\nabla}\cdot\vec{U}=0$, because h is assumed to be a constant equal to the pillar height. In other words, the velocity potential ϕ satisfies the Laplace equation

$$\nabla^2\phi=0, \quad (23)$$

where the boundary condition is determined from the continuity of the normal velocity and the pressure jump at the moving front of the liquid:

$$\vec{n}\cdot\vec{U}=U_0, \quad (24)$$

$$p=p_0+\gamma C, \quad (25)$$

where U_0 and C are the normal velocity and the curvature at the moving front; the curvature C is given, for example, by the sum of the curvature in the r-θ plane and that in the r-z plane: $C=C_{r\theta}+C_{rz}$.

For a circular moving front of radius R, the interface velocity is given by $U_0=\dot{R}$ where the dot stands for the time derivative; the local shape of the actual interface may be delicate, but, since our basic equation (21) tacitly assumes that physical quantities are z-independent, we seek a solution with a simplest boundary shape which is natural on a macroscopic scale: the unit vector normal to the front is given by $\vec{n}=(1,0,0)$ in the (r,θ,z) coordinate and the curvature is given by $C=C^{(0)}\equiv 1/R+C_{rz}$. Here, to be compatible with the arguments deriving eqs. (6) and (7), the second curvature C_{rz} should be set as

$$C_{rz}=C_0, \quad (26)$$

which is larger than $1/R$, so that eq. (25) reduces to eq. (7) as desired [24].

The solution to the Laplace equation satisfying the present θ-independent boundary condition is given in the form $\phi\equiv\phi^{(0)}=A\log(r/R)+B$, where A and B are determined by the boundary conditions; we find

$$\phi^{(0)}=\dot{R}R\log\frac{r}{R}+\kappa\left(\frac{\rho\omega^2R^2}{2}-p_0+p_c\right). \quad (27)$$

Since A has to be a constant for spatial coordinates, the front velocity $\dot{R}$ can be expressed as

$$\dot{R}=\frac{Q}{2\pi hR}, \quad (28)$$

where Q and h are space-independent. The pressure distribution for a circular interface $r=R$ is given from eqs. (27) and (22)

$$p^{(0)}(r)=p_0-p_c-\frac{\rho\omega^2}{2}(R^2-r^2)+\frac{\dot{R}}{\kappa}R\log\frac{R}{r}. \quad (29)$$

Practically, to maintain the constant film thickness h with the film expanding, we need to feed liquid; for example, we place a tube of radius r_c at the center of the film and control the central pressure to a value $p_0+\Delta$ (note that from the arguments in sect. 2, the maximum of Δ should be zero). In such a case, the front velocity $\dot{R}$

in eqs. (27) and (29) is not a direct controlling parameter but is passively determined by the boundary condition $p^{(0)}(r_c) = p_0 + \Delta$, which determines $\dot{R}$,

$$\frac{\dot{R}}{\kappa} R \log \frac{R}{r_c} = \frac{\rho\omega^2}{2}(R^2 - r_c^2) + p_c + \Delta. \tag{30}$$

The expression for $p^{(0)}(r)$ in eq. (29) with $\dot{R}$ given by eq. (30), which contains a constant term and terms proportional to $+r^2$ and to $-\log r$, has a minimum

$$r^*/R = \sqrt{\frac{\dot{R}/\kappa}{\rho\omega^2 R}}, \tag{31}$$

if $r^*/R < 1$ (in a practical parameter range where R/r_c is 10 to 100, we can assume $r^* > r_c$). However, if this is the case, the minimum should be lower than $p^{(0)}(R) = p - p_c$, which is not allowed if we remind the discussion in sect. 2; pressure inside the film cannot be lower than $p - p_c$. This leads to a condition, $r^*/R > 1$, or equivalently, the condition

$$\dot{R}/\kappa > \rho\omega^2 R. \tag{32}$$

In summary, the pressure deviation, $p^{(0)}(r) - p_0$, monotonously decreases from the maximum Δ at $r = r_c$ to the minimum $-p_c$ at $r = R$.

At this point, the relevance of eq. (26) can be shown from another point of view: this equation must hold for the present theory to be consistent with the previous theory. When $\omega = \Delta = 0$ and $r_c \lesssim R$ (and R is large), the velocity given in eq. (30) should recover the result obtained in the penetration theory discussed in appendix A from viewpoints different form the original work [17]. This is guaranteed by the above setting in eq. (26); putting $R = r_c + \eta$ in eq. (30), we obtain

$$\dot{\eta}\eta/\kappa = p_c, \tag{33}$$

which reduces to eq. (A.4) with eq. (A.6). Note also here some remarks on differences from previous studies in [26].

Let us now consider the case when the circular moving front $r = R$ is deformed to $r = \zeta \equiv R + \varepsilon(t)e^{in\theta}$; the unit normal vector $\vec{n} \propto \vec{\nabla}(r - \zeta)$ is given to first order in ε by $\vec{n} = (1, -\partial_\theta\zeta/R, 0)$ in the (r, θ, z) coordinate; the normal velocity of front is given to first order in ε by $U_0 = \vec{n} \cdot (\mathrm{d}\zeta/\mathrm{d}t, 0, 0) \simeq \mathrm{d}\zeta/\mathrm{d}t$. In this way, we obtain

$$U_0 = \dot{R} + \dot{\varepsilon}e^{in\theta}. \tag{34}$$

A possible solution to the Laplace equation now with a θ-dependent boundary condition is given in the form $\phi = \phi^{(0)} + D(r/R)^n e^{in\theta} + E$, where D and E are determined by the boundary condition. We find D from eq. (24)

$$nD = R\dot{\varepsilon} + \dot{R}\varepsilon. \tag{35}$$

Under this deformation of the rim ($r = \zeta$), the curvature $C_{r\theta}$ is modified from $1/R$ and calculated as $|\vec{\nabla} \cdot \vec{n}|$ while C_{rz} is unchanged. From eq. (35) and eq. (25), we obtain $E = 0$ and the equation

$$\frac{\dot{\varepsilon}}{\varepsilon} = -\frac{\dot{R}}{R}(n+1) + \kappa n \left[\rho\omega^2 - \frac{\gamma}{R^3}(n^2 - 1)\right]. \tag{36}$$

In the Poiseuille regime, this reduces to eq. (10) of ref. [23].

For large n, with the wave number $q = n/R$, we find

$$\frac{\dot{\varepsilon}}{\varepsilon} \propto -\dot{R}/\kappa + \rho\omega^2 R - \gamma q^2. \tag{37}$$

The scaling structure of the right-hand side reflects that of eq. (21): the first, the second and the third terms on the right-hand side of eq. (37) stand for the effects of viscosity, centrifugal force, and surface tension, respectively; when the right-hand side is positive, the mode is unstable; the centrifugal force is the source of destabilization while viscosity and capillarity tend to suppress the instability. Note, however, that $\dot{R}$ in eq. (37) is not a parameter controllable in experiment but is determined by centrifugal force and surface tension as seen in eq. (30). In this sense, the dynamics is determined essentially as a competition of centrifugal and surface forces.

The fastest-growing mode, for example for large n, can be found by minimizing the right-hand side of eq. (36) with respect to q after replacing R with n/q. As a matter of fact, however, from eq. (32), the left-hand side of eq. (37) is always negative: the instability is not expected. The physical reason is that, in order to keep the film thickness constant, the rotation speed cannot be too large; the effect of rotation which likes instability cannot be stronger than that of capillary which likes stability; as a result, instability disappears. However, when we put a plate on top of a texture surface to fabricate a Hele-Shaw cell with a forest of pillars inside, instability caused by rotation can appear; in such a case the pressure tuning is attained not by the pillar's top edges but by the two plates of the cell: in practice no upper bound like p_c exists in such a case.

The expression for velocity in eq. (30) might be able to be compared with experiments (although it is not directly related to instability). As already discussed, this reproduces the penetration laws derived in [17] when the rotation is absent. For a typical parameter set ($\rho = 10^3\,\mathrm{kg/m^3}$, $\omega = 10\,\mathrm{Hz}$, $R = 1\,\mathrm{cm}$, $\gamma = 20\,\mathrm{mN/m}$, $\eta = 10\,\mathrm{mPa\,s}$, $b = 2\,\mu\mathrm{m}$ and h or $l \sim 10\,\mu\mathrm{m}$), the second capillary term on the right-hand side is dominant and the front velocity $\dot{R}$ is around $0.3\,\mathrm{mm/s}$. As understood from eq. (32) which can be expressed as $\Delta + p_c > \rho\omega^2 R^2(\log R/r_c - 1/2)$, we cannot observe the regime where the rotation effect is dominant because there the film cannot keep its thickness. However, this implies that if we try to increase the rotation speed, the disk radius R is tuned to a critical value $R = R_c$ determined by

$$\rho\omega^2 R_c^2 = \frac{\Delta + p_c}{\log R_c/r_c - 1/2}. \tag{38}$$

In addition, this critical disk thus obtained is stable as seen above. This point would be interesting to be compared with experiments; *e.g.*, the critical radius of the disk gets smaller with increase in the angular velocity [27] (note that a film of molecular thickness can be developed outside the critical radius).

The above discussion up to eq. (36) actually includes the situation in the previous sections. The situation in sect. 4 corresponds to the case where the centrifugal term is absent and the sign of the velocity $\dot{R}$ is reversed (in the case of spin coating the liquid occupies the region $r < R$, while in the case of sect. 4 the region $r > R$); here, the source of instability is viscosity which is opposed by capillary

$$\frac{\dot{\varepsilon}}{\varepsilon} \simeq \dot{R}q/\kappa - \gamma q^3 \tag{39}$$

and the fastest mode is given by

$$3\gamma \left(\frac{2\pi}{\lambda}\right)^2 = \dot{R}/\kappa, \tag{40}$$

from which we obtain eq. (14) for the circular geometry (with U replaced with $\dot{R}$), or eq. (19). The case in sect. 3 corresponds to the case where $\omega = 0$, $R \to \infty$ and $Q \to \infty$, with $\dot{R} = Q/(2\pi hR)$ to be a finite value U to find eq. (39) but with $\dot{R}$ replaced with U, which leads to eq. (14). Note that in eqs. (36) and (37), $\dot{R}$ and R can be time-dependent; we do not have to keep the velocity $\dot{R}$ to be time-independent in experiments, as mentioned before. Likewise, U in sect. 3 is not necessarily time-independent.

6 Conclusion

We considered instability of liquid film moving on textured surfaces in different situations. We discuss the instability of receding film both when the receding edge is a straight line and a circular curve; we find scaling laws to be checked in future experiments in eqs. (14) and (19).

When the film is expanding via centrifugal force, we determine nontrivial boundary conditions by the original arguments given in sect. 2, which are summarized below. As a result, we find that instability is suppressed and find that the film may attain a critical state for strong rotation speed, for which we propose an equation to be checked with experiments in eq. (38). The physical reason for the disappearance of instability is as follows: the physical origin of a constant film thickness is capillary force which opposes instability and if centrifugal force which likes instability exceeds capillary force as we go away from the center the film terminates; as a result inside the film the effect of the capillary force always exceeds that of the centrifugal force so that instability is suppressed.

In sect. 2, we could give insights on the curvature of the edge of the moving film and the origin of constant film thickness: the film thickness is kept fixed because the top edges of pillars lift up the free surface of the film against the pressure drop inside the film; since the maximum lift-up force a single pillar can apply on the liquid surface is $2\pi b\gamma\cos\theta$, with $0 < \theta < \pi/2$ when the contact angle is zero, the force for a forest of pillars on the textured substrate where the pillars are arranged in the square lattice with lattice constant l should be in the range between 0 and $p_c = 2\pi b\gamma/l^2$ per unit area; the pressure p inside the film pinned by the pillars should be in the range, $p_0 - p_c < p < p_0$; in other words, the film on the textured surface should disappear when the inside pressure goes outside of this range.

In this paper, we have assumed that the effect of pinning and depinning from each pillar is not important to explain the macroscopic viscous dynamics on textured surfaces because this fact is established experimentally [17]; however, theoretical understanding on this is an important topic, which will be discussed elsewhere.

K.O. is grateful for David Quéré for useful discussions. He also thanks MEXT, Japan for KAKENHI.

Appendix A.

To estimate the curvature of the edge of the film moving on the textured surface, we discuss a penetrating film. We start from the classical Washburn law describing the dynamics of the capillary rise to see that the curvature of the front (which is known in this simple case) can be recovered by comparing derivations from different viewpoints. The first viewpoint is pressure; when a liquid column is advancing from a liquid bath in the z-direction via capillary tube of radius ρ, the lubricant equation $\partial p/\partial z = \eta\nabla^2 U$ is dimensionally estimated as

$$\frac{\gamma C}{z} \simeq \eta\frac{U}{\rho^2}, \tag{A.1}$$

where C is the curvature at the front; since $U = \mathrm{d}z/\mathrm{d}t$, eq. (A.1) results in the well-known Washburn law

$$z^2 = Dt, \quad \text{with} \quad D \simeq \gamma C\rho^2/\eta; \tag{A.2}$$

here, we know $C = 2/\rho$ from a geometrical condition when the contact angle at the front is zero but this can be "derived" by comparing the above result with that by the second derivation. The second derivation is from the energetic viewpoint; dissipation mainly occurs in the moving liquid column of volume $\pi\rho^2 z$; dissipation per unit time can be estimated as $\pi\rho^2 z \cdot \eta(U/\rho)^2$ for the liquid column, which should be balanced by the surface energy gain per unit time, $\mathrm{d}E/\mathrm{d}t = (\gamma_{SL} - \gamma_S)2\pi\rho\mathrm{d}z/\mathrm{d}t = 2\pi\gamma\rho U$ because the contact angle is assumed to be zero; from the balancing equation we obtain, writing the correct numerical coefficient,

$$z^2 = \gamma\rho t/(2\eta); \tag{A.3}$$

comparing this with eq. (A.2) we rediscover the curvature $2/\rho$. (The third viewpoint is force; the moving liquid column is lifted upwards at the top by a surface tension with a force $f_1 = 2\pi\rho\gamma_S$, while dragged downwards at the bottom with a force $f_2 = 2\pi\rho\gamma_{SL}$; the net capillary force $f_1 - f_2 = 2\pi\rho\gamma$ should be balanced by a viscous force $8\pi\eta(U/\rho)\rho z$ (note that pressures on the liquid column at slightly above the top and at the bottom are both p_0), which leads to again eq. (A.3).)

For a penetrating film on a textured substrate, eq. (A.1) based on the pressure viewpoint is replaced with

$$\frac{\gamma C}{z} \simeq \dot{z}/\kappa, \tag{A.4}$$

so that we obtain

$$z^2 = Dt, \quad \text{with} \quad D \simeq \gamma\kappa C. \tag{A.5}$$

From the energetic viewpoint, dissipation per unit length of the moving film of volume zh can be estimated as per unit time, $zh \cdot \eta(U/L)^2$, with L defined in eq. (14), which should be balanced by the surface energy gain per unit time; the energy gain for displacement of the front by $\mathrm{d}z$ is given as $\mathrm{d}E = \gamma \mathrm{d}z + r(\gamma_{SL} - \gamma_S)\mathrm{d}z$, with $\gamma = \gamma_S - \gamma_{SL}$, where the roughness parameter r is given by $(2\pi bh + l^2)/l^2$: the change per unit time is given by $\mathrm{d}E/\mathrm{d}t \simeq 2\pi bh\gamma U/l^2$; then, balancing the dissipation and energy, we obtain the result obtained in [17] from the force viewpoint: $z^2 \simeq \gamma\kappa t \cdot 2\pi b/l^2$; comparing this with eq. (A.5), we obtain

$$C \simeq 2\pi b/l^2 \tag{A.6}$$

in both the Poiseuille and Stokes regime. The third force viewpoint is discussed in the original paper [17].

This result for the curvature for the film on the textured surfaces can be interpreted in the following way. At the advancing front the pressure is lower than the atmospheric pressure p_0 by the amount $p_c = \gamma C$ and this pressure drop drives the liquid film.

References

1. P.G. De Gennes, F. Brochard-Wyart, D. Quéré, *Gouttes, Bulles, Perles et Ondes* (Belin, Paris, 2002).
2. J. Bico, C. Tordeux, D. Quéré, Europhys. Lett. **55**, 214 (2001).
3. M. Callies, D. Quéré, Soft Matter **1**, 55 (2005).
4. A. Otten, S. Herminghaus, Langmuir **20**, 2405 (2004).
5. R. Narhe, D. Beysens, Phys. Rev. Lett. **93**, 076103 (2004).
6. M. Tasinkevych, S. Dietrich, Phys. Rev. Lett. **97**, 106102 (2006).
7. L. Courbin, E. Denieul, E. Dressaire, M. Roper, A. Ajdari, H.A. Stone, Nat. Mater. **6**, 661 (2007).
8. N.A. Patanker, Langmuir **19**, 1249 (2003).
9. A. Marmur, Langmuir **19**, 8343 (2003).
10. C. Ishino, K. Okumura, D. Quéré, Europhys. Lett. **68**, 419 (2004).
11. C. Ishino, K. Okumura, Europhys. Lett. **76**, 464 (2006).
12. C. Ishino, K. Okumura, Eur. Phys. J. E **25**, 415 (2008).
13. A. Dupuis, J.M. Yeomans, Langmuir **21**, 2624 (2005).
14. H. Kusumaatmajya, J.M. Yeomans, Langmuir **23**, 6019 (2007).
15. S. Moulinet, D. Bartolo, Eur. Phys. J. E **24**, 251 (2007).
16. M. Reyssat, J.M. Yeomans, D. Quéré, EPL **81**, 26006 (2008).
17. C. Ishino, M. Reyssat, E. Reyssat, K. Okumura, D. Quéré, EPL **79**, 56005 (2007).
18. P.G. Saffman, G. Taylor, Proc. R. Soc. London, Ser. A **245**, 312 (1958).
19. E. Guyon, J.-P. Hulin, *Hydrodynamique Physique* (Paris, CNRS Éditions, 2001).
20. H. Hasimoto, J. Fluid Mech. **5**, 317 (1959).
21. F. Melo, J.F. Joanny, S. Fauve, Phys. Rev. Lett. **63**, 1958 (1989).
22. L. Paterson, J. Fluid Mech. **113**, 513 (1981).
23. L. Carrillo *et al.*, Phys. Rev. E **54**, 6260 (1996).
24. In the present case the determination of C_{rz} is delicate from a geometrical point of view but we can determine C_{rz} in this way, while in [25] and [23] the authors assumed essentially $C_{rz} = 0$ in order to derive a solution to a non-fluctuating straight advancing front line and in [18] and [22] the authors assumed that $1/C_{rz}$ is determined by the cell thickness from a geometrical viewpoint.
25. H.E. Huppert, Nature **300**, 427 (1982).
26. In the usual case of spin coating where the film becomes thinner as it expands, the z-independent pressure p inside the liquid in eq. (21) can be set as the sum of the atmospheric pressure and the Laplace pressure jump due to the curvature of the film surface: $p(r,\theta) = p_0 + \gamma\nabla^2 h(r,\theta)$ in the region with weak curvatures [21]. However, in the present case, as in the cases of the spinning Hele-Shaw cell [22,23], we cannot use this setting of pressure because the film thickness is assumed to be a constant (*i.e.*, h is equal to the pillar height) on a sub-macroscopic scale: in the case of Hele-Shaw cell and in the present case the plate and pillars can tune pressure on the liquid as discussed in sect. 2, respectively.
27. If we could increase Δ, the spin coating could be performed up to a larger R without causing instability, which would be useful in industry. Unfortunately, the maximum of Δ is zero, as mentioned above.